

The effect of different observational data on the constraints of cosmological parameters

Yungui Gong,^{1,2,3*} Qing Gao,^{1†} and Zong-Hong Zhu,^{4‡}

¹College of Mathematics and Physics, Chongqing University of Posts and Telecommunications, Chongqing 400065, China

²MOE Key Laboratory of Fundamental Quantities Measurement, School of Physics, Huazhong University of Science and Technology, Wuhan 430074, China

³Institute of Theoretical Physics, Chinese Academy of Sciences, Beijing 100190, China

⁴Department of Astronomy, Beijing Normal university, Beijing 100875, China

5 March 2018

ABSTRACT

The constraints on the Λ cold dark matter (Λ CDM) model from type Ia supernova (SNe Ia) data alone and BAO data alone are similar, so it is worthwhile to compare their constraints on the property of dark energy. We apply the three-year Supernova Legacy Survey (SNLS3) compilation of 472 SNe Ia data, the baryon acoustic oscillation measurement of distance, the cosmic microwave background radiation data from the seven-year *Wilkinson Microwave Anisotropy Probe* (WMAP7), and the Hubble parameter data to study the effect of their different combinations on the fittings of cosmological parameters in the modified holographic dark energy model and the Chevallier-Polarski-Linder model. Neither BAO nor WMAP7 data alone give good constraint on the equation of state parameter of dark energy, but both WMAP7 data and BAO data help SNe Ia data break the degeneracies among the model parameters, hence tighten the constraint on the variation of equation of state parameter w_a , and WMAP7 data do the job a little better. Although BAO and WMAP7 data provide reasonably good constraints on Ω_m and Ω_k , they are not able to constrain the dynamics of dark energy. On the other hand, SNe Ia data do not provide good constraints on Ω_m and Ω_k , but they provide good constraint on the dynamics of dark energy, especially the variation of the equation of state parameter of dark energy, so we need to combine SNe Ia with BAO and WMAP7 data to probe the property of dark energy. The addition of $H(z)$ data helps better constrain the geometry of the Universe Ω_k and the property of dark energy. For the SNLS SNe Ia data, the nuisance parameters α and β are consistent for all different combinations of the above data, and their impacts on the fittings of cosmological parameters are minimal. By fitting the data to different models, Λ CDM model is still consistent with all the observational data.

Key words: cosmology: theory; dark energy; cosmological parameters

1 INTRODUCTION

The accelerating expansion of the Universe was first discovered in 1998 by the observations of Type Ia supernovae (SNe Ia) (Riess et al. 1998; Perlmutter et al. 1999). As more accurate data are available, it is possible to measure the acceleration and the dynamical mechanism behind the acceleration. There are three different possibilities for the acceleration. The first possibility is that a new exotic form of matter with negative pressure, dubbed as dark energy drives the Universe to accelerate. The cosmological constant is the simplest candidate of dark energy which is also consistent with observations, but at odds with quantum field theory. The second possibility is that general relativity is modified at the cosmological scale, such as Dvali-Gabadadze-Porrati (DGP) model

(Dvali, Gabadadze & Porrati 2000). The third possibility is that the Universe is inhomogeneous. In this paper, we consider the possibility of dark energy only.

In the recent release of the measurements of the baryon acoustic oscillation (BAO) peaks at redshifts $z = 0.44, 0.6$ and 0.73 in the galaxy correlation function of the final data set of the WiggleZ dark energy survey, Blake et al. (2011) used these three BAO data along with the BAO data at redshifts $z = 0.2$ and 0.35 measured from the distribution of galaxies (Percival et al. 2010) and the measurement of BAO at redshift $z = 0.106$ from the six-degree Field Galaxy Survey (6dFGS) (Beutler et al. 2011) to constrain Λ cold dark matter (Λ CDM) model. It was found that the constraints on Λ CDM model from the BAO data are even better than those from Union2 SNe Ia data (Amanullah et al. 2010). Blake et al. (2011) also found that the combination of BAO and the seven-year *Wilkinson Microwave Anisotropy Probe* (WMAP7) data gives much better constraints on Λ CDM model than the combination of SNe Ia

* yggong@mail.hust.edu.cn

† gaoqing01good@163.com

‡ zhuzh@bnu.edu.cn

and WMAP7 data does. This means that the updated BAO data (Blake et al. 2011) are robust to constrain cosmological parameters. If the constraints on the property of dark energy from BAO data are much tighter than those from SNe Ia data, then we just need to apply BAO data only for a faster fitting although SNe Ia data and BAO data are complementary to each other. The redshifts of BAO data span from $z = 0.106$ to $z = 0.73$, we may expect that BAO data catch the dynamical property of dark energy, so it is necessary to study the effects of different observational data and their combinations on the constraints on the equation of state of dark energy. In this paper, we use a simple dark energy model to test the robustness of BAO data, and compare the constraints on the equation of state of dark energy from different data.

The question whether dark energy is just the cosmological constant remains to be answered. Recently, there are lots of studies in determining whether Λ CDM model is consistent with observations (Huang et al. 2009; Shafieloo, Sahni & Starobinsky 2009; Cai, Su & Zhang 2010; Lampeitl et al. 2009; Serra et al. 2009; Gong et al. 2010; Gong, Wang & Cai 2010; Pan et al. 2010; Gong, Zhu & Zhu 2011; Li et al. 2011). Through the reconstruction of $Om(z) = [E^2(z) - 1]/[(1+z)^3 - 1]$ with the dimensionless Hubble parameter $E(z) = H(z)/H_0$ (Sahni, Shafieloo & Starobinsky 2008), Li, Wu & Yu (2011) considered the tensions between different data set by using Chevallier-Polarski-Linder (CPL) parametrization (Chevallier & Polarski 2001; Linder 2003) of the equation of state of dark energy. They found that a tension between low redshift and high redshift data existed. Su, Tuo & Cai (2011) used the figure of merit (FOM) proposed by the Dark Energy Task Force (Albrecht et al. 2006) as a diagnostic to study the effectiveness of different combinations of data on constraining w_0 and w_a in CPL model.

In this paper, we first study the robustness of BAO data, then study the constraints on the equation of state of dark energy based on different combinations of the following data: the three-year Supernova Legacy Survey (SNLS3) sample of 472 SNe Ia data with systematic errors (Conley et al. 2011); the BAO measurements from the 6dFGS (Beutler et al. 2011), the distribution of galaxies (Percival et al. 2010) in the Sloan Digital Sky Survey (SDSS) and the WiggleZ dark energy survey (Blake et al. 2011); the WMAP7 data (Komatsu et al. 2011); and the Hubble parameter $H(z)$ data (Gaztanaga, Cabre & Hui 2009; Stern et al. 2010). In addition to studying the effects of different observational data and their combinations on the constraints of cosmological parameters, we also reconstruct the equation of state of dark energy $w(z)$, the deceleration parameter $q(z)$ and $Om(z)$ by using these data sets. On the other hand, the distance measurements from SNe, BAO and WMAP7 data depend on $w(z)$ through double integrations, the process of double integrations smoothes out the variation of $w(z)$. Since the Hubble parameter $H(z)$ depends on $w(z)$ through a single integration, the Hubble parameter $H(z)$ can detect the variation of $w(z)$ better than the distance scales and needs to be applied to fit cosmological models.

The paper is organized as follows. In section 2, we present the SNLS3 SNe Ia data (Conley et al. 2011), the BAO data (Beutler et al. 2011; Blake et al. 2011; Percival et al. 2010), the WMAP7 data (Komatsu et al. 2011), the $H(z)$ data (Gaztanaga, Cabre & Hui 2009; Stern et al. 2010), and all the formulae related to these data. In section 3, we present all the models and the fitting results, and conclusions are drawn in section 4.

2 OBSERVATIONAL DATA

2.1 SNe Ia data

The SNLS3 SNe Ia data consist of 123 low-redshift SNe Ia data with $z \lesssim 0.1$ mainly from Calan/Tololo, CfAI, CfAII, CfAIII and CSP, 242 SNe Ia over the redshift range $0.08 < z < 1.06$ observed from the SNLS (Conley et al. 2011), 93 intermediate-redshift SNe Ia data with $0.06 \lesssim z \lesssim 0.4$ observed during the first season of Sloan Digital Sky Survey (SDSS)-II supernova (SN) survey (Kessler et al. 2009), and 14 high-redshift SNe Ia data with $z \gtrsim 0.8$ from *Hubble Space Telescope* (Riess et al. 2007). The SNLS3 SNe Ia data used the combination of SALT2 and SiFTO light-curve fitters (Conley et al. 2011). To use the 472 SNLS3 SNe Ia data (Conley et al. 2011), we minimize

$$\chi_{sn}^2(\mathbf{p}, \alpha, \beta) = \sum_{i,j=1}^{472} (m_B - m_{mod})^T C_{sn}^{-1} (m_B - m_{mod}), \quad (1)$$

where m_B is the rest-frame peak B-band magnitude of a SN, the predicted magnitude of the SN given a cosmological model is $m_{mod} = 5 \log_{10} \mathcal{D}_L(z_{hel}, z_{cmb}, \mathbf{p}) - \alpha(s - 1) + \beta \mathcal{C} + \mathcal{M}_B$, z_{hel} and z_{cmb} are the heliocentric and the CMB frame redshifts of the SN, s is the stretch given by the data, \mathcal{C} is the color measure for the SN given by the data, α and β are nuisance parameters used for the SNLS3 data fitting, \mathcal{M}_B is another nuisance parameter incorporating the absolute magnitude and Hubble constant and it is marginalized over in the SNe data fitting process because of the arbitrary normalization of the magnitude, $C_{sn}(z_i, z_j)$ is the covariant matrix which includes both the systematical and statistical uncertainties for the SNe Ia data (Conley et al. 2011). The correction on the dependence of the host-galaxy stellar mass is also included. The Hubble-constant free luminosity distance $\mathcal{D}_L(z)$ is

$$\mathcal{D}_L(z) = H_0 d_L(z) = \frac{1+z}{\sqrt{|\Omega_k|}} S_k \left[\sqrt{|\Omega_k|} \int_0^z \frac{dx}{E(x)} \right], \quad (2)$$

where the dimensionless Hubble parameter $E(z) = H(z)/H_0$ and $S_k(x)$ is defined as x , $\sin(x)$ or $\sinh(x)$ for $k = 0, +1$, or -1 , respectively. For the fitting to the SNLS3 data, we need to add two more nuisance parameters α and β in addition to the model parameters \mathbf{p} and the nuisance parameter \mathcal{M}_B .

2.2 BAO data

For the BAO data, we use the measurements from the 6dFGS (Beutler et al. 2011), the distribution of galaxies (Percival et al. 2010) in the SDSS and the WiggleZ dark energy survey (Blake et al. 2011). Percival et al. (2010) measured the distance ratio,

$$d_z = \frac{r_s(z_d)}{D_V(z)} \quad (3)$$

at two redshifts $z = 0.2$ and $z = 0.35$ by fitting to the power spectra of luminous red galaxies and main-sample galaxies in the SDSS. Here the effective distance is

$$D_V(z) = \left[\frac{d_L^2(z)}{(1+z)^2} \frac{z}{H(z)} \right]^{1/3}, \quad (4)$$

the drag redshift z_d is (Eisenstein & Hu 1998),

$$z_d = \frac{1291(\Omega_m h^2)^{0.251}}{1 + 0.659(\Omega_m h^2)^{0.828}} [1 + b_1(\Omega_b h^2)^{b_2}], \quad (5)$$

Table 1. The BAO distance data from the 6dFGS (Beutler et al. 2011), SDSS (Percival et al. 2010) and WiggleZ surveys (Blake et al. 2011).

Data	z	d_z	$A(z)$
6dFGS	0.106	0.336 ± 0.015	
SDSS	0.2	0.1905 ± 0.0061	
SDSS	0.35	0.1097 ± 0.0036	
WiggleZ	0.44		0.474 ± 0.034
WiggleZ	0.6		0.442 ± 0.020
WiggleZ	0.73		0.424 ± 0.021

where

$$b_1 = 0.313(\Omega_m h^2)^{-0.419} [1 + 0.607(\Omega_m h^2)^{0.674}], \quad (6)$$

$$b_2 = 0.238(\Omega_m h^2)^{0.223}, \quad (7)$$

the comoving sound horizon is

$$r_s(z) = \int_z^\infty \frac{c_s(x) dx}{H(x)}, \quad (8)$$

the sound speed $c_s(z) = 1/\sqrt{3[1 + \bar{R}_b/(1+z)]}$, and $\bar{R}_b = 3\Omega_b h^2/(4 \times 2.469 \times 10^{-5})$. Beutler et al. (2011) derived that $d_{0.106}^{obs} = 0.336 \pm 0.015$ from the 6dFGS measurements. The WiggleZ dark energy survey measured the acoustic parameter

$$A(z) = \frac{D_V(z) \sqrt{\Omega_m H_0^2}}{z}, \quad (9)$$

at three redshifts $z = 0.44$, $z = 0.6$ and $z = 0.73$. To use the BAO data, we minimize

$$\begin{aligned} \chi_{Bao}^2(\mathbf{p}, \Omega_b h^2, h) &= \sum_{i,j=1}^2 \Delta d_i C_{dz}^{-1}(d_i, d_j) \Delta d_j \\ &+ \frac{(d_{0.106} - 0.336)^2}{0.015^2} \\ &+ \sum_{i,j=1}^3 \Delta A_i C_A^{-1}(A_i, A_j) \Delta A_j, \end{aligned} \quad (10)$$

where $d_i = (d_{z=0.2}, d_{z=0.35})$, $\Delta d_i = d_i - d_i^{obs}$ and the covariance matrix $C_{dz}(d_i, d_j)$ for d_z at $z = (0.2, 0.35)$ is taken from equation (5) in Percival et al. (2010); $A_i = (A(0.44), A(0.6), A(0.73))$, $\Delta A_i = A(z_i) - A(z_i)^{obs}$ and the covariance matrix $C_A(A_i, A_j)$ for the data points $A(z)$ at $z = (0.44, 0.6, 0.73)$ is taken from table 2 in Blake et al. (2011). The BAO data listed in Table 1 span the redshift regions 0.106 – 0.73 in which dark energy is supposed to dominate cosmic expansion, so we naively expect that the BAO data can catch the dynamics of dark energy. Besides the model parameters \mathbf{p} , we need to add two more nuisance parameters $\Omega_b h^2$ and $\Omega_m h^2$ when we use the BAO data from 6dFGS (Beutler et al. 2011) and SDSS (Percival et al. 2010).

2.3 WMAP7 data

For the WMAP7 data, we use the measurements of the three derived quantities: the shift parameter $R(z^*)$ and the acoustic index $l_A(z^*)$ at the recombination redshift z^* . The shift parameter R is expressed as

$$R(z^*) = \frac{\sqrt{\Omega_m} \mathcal{D}_L(z^*)}{1+z^*}. \quad (11)$$

The acoustic index l_A is

Table 2. The maximum likelihood (ML) and the inverse covariance matrix for the three distance priors (Komatsu et al. 2011).

x_i	l_A	R	z^*	ML
l_A	2.305	29.698	-1.333	302.09
R		6825.270	-113.180	1.725
z^*			3.414	1091.3

$$l_A(z^*) = \frac{\pi d_L(z^*)}{(1+z^*) r_s(z^*)}, \quad (12)$$

and the recombination redshift z^* is fitted by (Hu & Sugiyama 1996),

$$z^* = 1048 [1 + 0.00124(\Omega_b h^2)^{-0.738}] [1 + g_1(\Omega_m h^2)^{g_2}], \quad (13)$$

$$g_1 = \frac{0.0783(\Omega_b h^2)^{-0.238}}{1 + 39.5(\Omega_b h^2)^{0.763}}, \quad g_2 = \frac{0.560}{1 + 21.1(\Omega_b h^2)^{1.81}}. \quad (14)$$

In particular, we minimize

$$\chi_{CMB}^2(\mathbf{p}, \Omega_b h^2, h) = \sum_{i,j=1}^3 \Delta x_i C_{CMB}^{-1}(x_i, x_j) \Delta x_j, \quad (15)$$

where the three parameters $x_i = [R(z^*), l_A(z^*), z^*]$, $\Delta x_i = x_i - x_i^{obs}$ and the covariance matrix $C_{CMB}(x_i, x_j)$ for the three parameters taken from table 10 in Komatsu et al. (2011) are listed in Table 2. We also need to add the nuisance parameters $\Omega_b h^2$ and $\Omega_m h^2$ to the parameter space when we fit the WMAP7 data.

2.4 Hubble data

The distances measured by the SNe, BAO and WMAP7 data depend on the double integrations of the equation of state parameter $w(z)$, the process of double integrations smoothes out the variation of equation of state parameter $w(z)$ of dark energy. However, the Hubble parameter $H(z)$ depends on one integration of $w(z)$. Therefore, the Hubble parameter $H(z)$ can detect the variation of $w(z)$ better than the distance scales do. Furthermore, it was found that $w(z)$ at high redshifts will be better constrained with the addition of $H(z)$ data (Gong et al. 2010). So we also use the $H(z)$ data at 11 different redshifts obtained from the differential ages of passively evolving galaxies (Simon, Verde & Jimenez 2005; Stern et al. 2010), and three more Hubble parameter data at redshifts $z = 0.24$, $z = 0.34$ and $z = 0.43$, determined by taking the BAO scale as a standard ruler in the radial direction (Gaztanaga, Cabre & Hui 2009). The $H(z)$ data span out to the redshift regions $z = 1.75$ and is shown in Table 3. So we add these $H(z)$ data to χ^2 ,

$$\chi_H^2(\mathbf{p}, h) = \sum_{i=1}^{14} \frac{[H(z_i) - H_{obs}(z_i)]^2}{\sigma_{hi}^2}, \quad (16)$$

where σ_{hi} is the 1σ uncertainty of $H(z)$.

2.5 Fitting method

Basically, the model parameters \mathbf{p} are determined by minimizing

$$\chi^2 = \chi_{sn}^2 + \chi_{Bao}^2 + \chi_{CMB}^2 + \chi_H^2. \quad (17)$$

The likelihood for the parameters \mathbf{p} in the model and the nuisance parameters is computed using the Monte Carlo Markov Chain

Table 3. The 14 $H(z)$ data from sources a (Stern et al. 2010), b (Simon, Verde & Jimenez 2005) and c (Gaztanaga, Cabre & Hui 2009).

z	$H(z)$ [km/sec/Mpc]	sources
0.1	69 ± 12	a
0.17	83 ± 8	a
0.27	77 ± 14	a
0.4	95 ± 17	a
0.48	97 ± 62	a
0.88	90 ± 40	a
0.9	117 ± 23	a
1.3	168 ± 17	b
1.43	177 ± 18	b
1.53	140 ± 14	b
1.75	202 ± 40	b
0.24	76.69 ± 2.32	c
0.34	83.8 ± 2.96	c
0.43	86.45 ± 3.27	c

(MCMC) method. The MCMC method randomly chooses values for the above parameters, evaluates χ^2 and determines whether to accept or reject the set of parameters using the Metropolis-Hastings algorithm. The set of parameters that are accepted to the chain forms a new starting point for the next process, and the process is repeated for a sufficient number of steps until the required convergence is reached. Our MCMC code is based on the publicly available package COSMOMC (Lewis & Bridle 2002; Gong, Wu & Wang 2008). When SNe Ia data are used, we also need to fit the two nuisance parameters α and β , when BAO or WMAP7 data are used, we need to fit the two nuisance parameters $\Omega_b h^2$ and $h = H_0/100$. So when we combine SNe Ia with BAO or WMAP7 data, we need to fit four nuisance parameters ($\alpha, \beta, \Omega_b h^2, h$).

After fitting the observational data to different dark energy models, we apply the Om diagnostic (Sahni, Shafieloo & Starobinsky 2008) to detect the deviation from the Λ CDM model. For the Λ CDM model with $\Omega_k = 0$ (we call flat model afterwards), $Om(z) = \Omega_m$ is a constant which is independent of the value of Ω_m . Because of this property, Om diagnostic is less sensitive to observational errors than the equation of state parameter $w(z)$ does. On the other hand, the bigger the value of $Om(z)$, the bigger the value of $w(z)$, so the behavior of $Om(z)$ catches the dynamical property of $w(z)$.

We also apply the FOM as a diagnostic tool to compare the effectiveness of different combinations of observational data on constraining the equation of state parameters w_0 and w_a in CPL model. FOM is defined as the reciprocal of the area of the error ellipse enclosing the 95% confidence limit in the w_0 - w_a plane, it is proportional to $[\det C_w(w_0, w_a)]^{-1/2}$, here $C_w(w_0, w_a)$ is the correlation matrix of w_0 and w_a .

3 COSMOLOGICAL FITTING RESULTS

3.1 Λ CDM model

We first review the effects of different combinations of observational data on the Λ CDM model with non-zero Ω_k (we call it curved model afterward). The Ω_m - Ω_Λ contour from applying only the SNLS3 SNe data was shown in figure 8 in Conley et al. (2011). By combining the SNLS3 SNe and the WMAP7 data, Sullivan et al. (2011) obtained the constraints on Ω_m and Ω_k , and

the contours were shown in figure 5 of their paper. From these results, we see that SNLS3 SNe data alone do not provide tight constraints on Ω_m and Ω_k . With the addition of WMAP7 data, the constraint on Ω_k becomes much tighter, so the constraint on Ω_m becomes tighter. Therefore, WMAP7 data can be used to tighten the constraint on the geometry of the Universe (Blake et al. 2011). By applying the BAO data only with the assumption that $\Omega_b h^2 = 0.02227$, Blake et al. (2011) found the constraints on Ω_m and Ω_k . Comparing the constraints from SNLS3 or Union2 SNe Ia data alone with those from BAO data alone, we see that the constraints are similar, and the constraint on Ω_m from BAO data alone is even much better than that from SNe Ia data alone. Blake et al. (2011) also compared the constraint on the curved Λ CDM model from the combinations of WMAP7 with BAO and Union2 SNe Ia data, and they found that Ω_m - Ω_k contours from the combination of BAO and WMAP7 data are smaller than those from the combination of Union2 SNe Ia and WMAP7 data. Moreover, the constraints from the combination of Union2 SNe Ia, BAO and WMAP7 data are similar to those from the combination of BAO and WMAP7 data. These results show that BAO data mainly tighten the constraint on Ω_m and WMAP7 data mainly tighten the constraint on Ω_k , while current SNe Ia data still give large Ω_m - Ω_k contours, so the addition of SNe data to the combination of BAO and WMAP7 data has little effect in improving the constraints of Ω_m and Ω_k . For comparison, we show all the constraints in Fig. 1. Note that we set the nuisance parameters $\Omega_b h^2$ and h as free parameters in fitting BAO and WMAP7 data, so we fit the four parameters ($\Omega_m, \Omega_k, \Omega_b h^2, h$) when BAO or WMAP7 data are used, the four parameters ($\Omega_m, \Omega_k, \alpha, \beta$) when SNe data are used, and six parameters ($\Omega_m, \Omega_k, \Omega_b h^2, h, \alpha, \beta$) when we combine SNe with BAO or WMAP7 data. In Fig. 1, we show the constraints on the curved Λ CDM model from SNLS3 SNe Ia data alone (the green lines), BAO data alone (the yellow line), the combination of SNLS3 SNe Ia and BAO data (the cyan lines), the combination of SNLS3 SNe Ia and WMAP7 data (the magenta lines), the combination of BAO and WMAP7 data (the blue lines), the combination of SNLS3 SNe Ia, BAO and WMAP7 data (the red lines) and the combination of all observational data (the shaded regions). In the left-hand panels, we use the following data: SNe data alone, BAO data alone, and the combination of SNe and BAO data. In the right-hand panels, we use the following data: the combination of SNe and WMAP7 data, the combination of BAO and WMAP7 data, the combination of SNe, BAO and WMAP7 data and all the data combined. These results are summarized in Table 4.

Although the binned SNe data measure the distance-redshift relation at $z < 0.8$ with three to four times higher accuracy than the BAO data (Blake et al. 2011), the constraints from SNe and BAO data are similar and BAO data constrain Ω_m even better. As it is well known, the directions of degeneracy between Ω_m and Ω_Λ from SNe and BAO data are different, so the combination of these two data sets can improve the accuracy of the constraints much better. However, the uncertainties on Ω_m and Ω_k constrained from the combination of BAO and WMAP7 data become much smaller than those from SNe data alone, so the addition of SNe data to the combination of BAO and WMAP7 data has little effect even though the degeneracy directions are different. The addition of $H(z)$ data further reduces the uncertainty of Ω_k and moves the best-fitting value of Ω_k towards zero. We also find that the uncertainties of the nuisance parameters α and β are around 0.1, and they are all consistent at 1σ level for different fittings.

By using the measurement of d_z at $z = 0.275$ from Percival et al. (2010), the Ω_m - Ω_Λ contours were plotted in figure

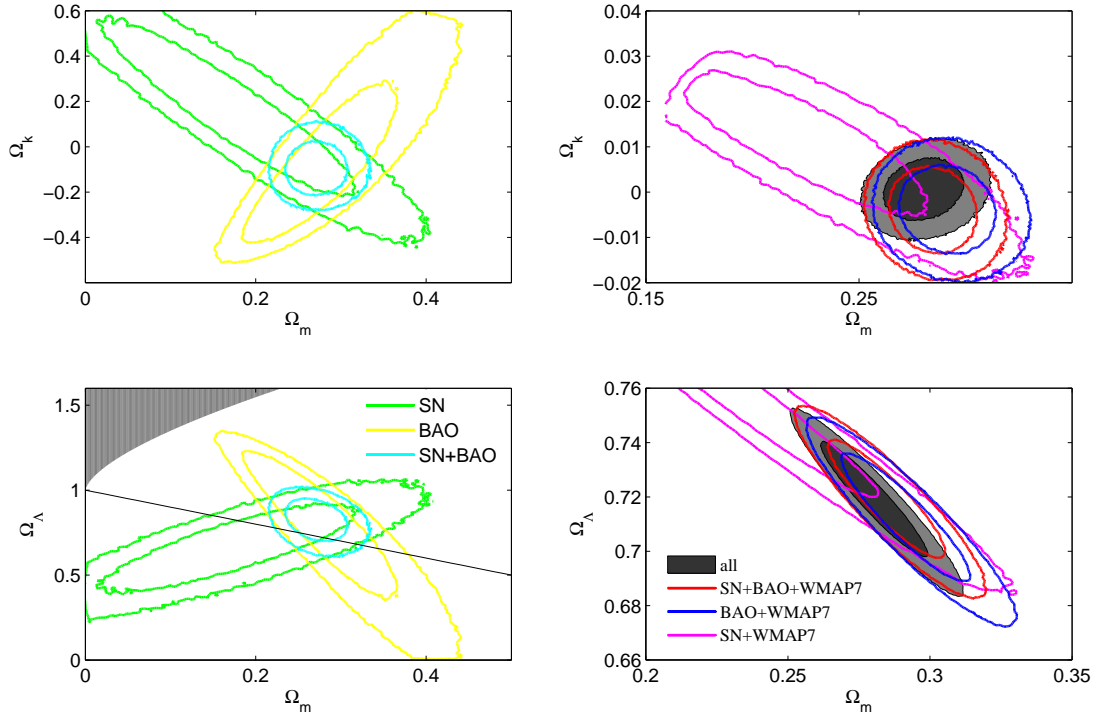


Figure 1. The marginalized 1σ and 2σ contour plots of Ω_m and Ω_k , and Ω_m and Ω_Λ for the curved Λ CDM model. In the left-hand panels, we use the following data: SNe data alone, BAO data alone, and the combination of SNe and BAO data. In the right-hand panels, we use the following data: the combination of SNe and WMAP7 data, the combination of BAO and WMAP7 data, and all the data combined. The green lines label the constraints from SNe Ia data only, the yellow lines label the constraints from BAO data only, the cyan lines label the constraints from the combination of SNe Ia and BAO data, the magenta lines label the constraints from the combination of SNe Ia and WMAP7 data, the blue lines label the constraints from the combination of WMAP7 and BAO data, the red lines label the constraints from the combination of SNe Ia, BAO and WMAP7 data, and the shaded regions label the constraints from the combination of all the observational data described in section 2. The black solid line the lower-left panel denotes the flat Λ CDM model.

Table 4. The marginalized 1σ errors for Ω_m and Ω_k in curved Λ CDM model constrained by different observational data

Data	Ω_m	Ω_k
SNe Ia	$0.17^{+0.1}_{-0.09}$	0.15 ± 0.25
BAO	$0.26^{+0.09}_{-0.03}$	$-0.16^{+0.38}_{-0.11}$
SNe+BAO	0.27 ± 0.02	$-0.11^{+0.09}_{-0.07}$
SNe+WMAP7	$0.22^{+0.05}_{-0.03}$	0.01 ± 0.01
BAO+WMAP7	$0.29^{+0.02}_{-0.01}$	$-0.004^{+0.007}_{-0.006}$
SNe+BAO+WMAP7	0.28 ± 0.01	$-0.004^{+0.006}_{-0.007}$
All	$0.28^{+0.02}_{-0.01}$	$0.0006^{+0.0046}_{-0.0045}$

5 in Percival et al. (2010) and figure 10 in Amanullah et al. (2010). Comparing those plots (Percival et al. 2010; Amanullah et al. 2010) with ours in Fig. 1, it is clear that the updated BAO data (Blake et al. 2011) greatly improve the constraints on Ω_m and Ω_Λ , and the ability of constraining the curved Λ CDM model by current BAO data (Blake et al. 2011) is even better than that by SNe Ia data. Therefore, it is interesting to study the ability of current BAO data

on constraining the dynamical behavior of dark energy. However, we need to understand what causes the improvement. We would like to see whether it is due to more data or larger redshift regions the data spanned. To do that, we compare the constraints on the curved Λ CDM model from individual BAO data. For the BAO data from SDSS (Percival et al. 2010) and 6dFGS (Beutler et al. 2011), there are two nuisance parameters $\Omega_b h^2$ and h in addition to the two model parameters Ω_m and Ω_k , so we need to impose priors to get some reasonable results. Following Percival et al. (2010), we fix $\Omega_b h^2 = 0.02227$ and consider both cases with $h = 0.738$ (Riess et al. 2011) and free h . The results are shown in Fig. 2. When h is a free parameter, Ω_m is not well constrained by the combination of 6dFGS and SDSS data (the magenta contours). However, when we take $h = 0.738$ (the cyan contours), the constraint on Ω_m is greatly improved. We also check the case with the prior $H_0 = 73.8 \pm 2.4$ (Riess et al. 2011), and the situation is similar although the improvement over free H_0 is smaller. For the BAO data from WiggleZ (Blake et al. 2011), we only have two model parameters Ω_m and Ω_k and the results are shown by the red contours in Fig. 2. We see that the constraints from WiggleZ data (the red contours) are similar to those from the combination of 6dFGS and SDSS with nuisance parameters fixed (the cyan contours) and the combination of 6dFGS, SDSS and WiggleZ data with free nuisance parameters (the blue contours), and these results are consistent with each other. We also check the constraints from one of the three

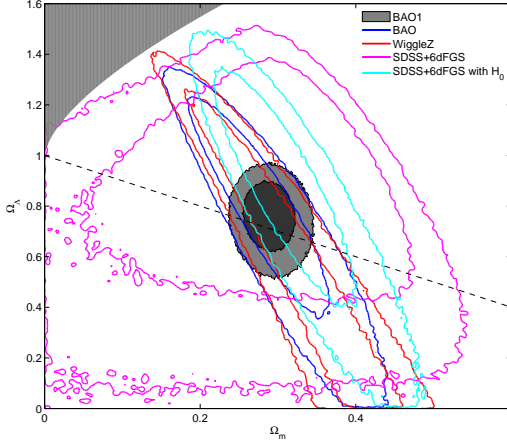


Figure 2. The marginalized 1σ and 2σ contour plots of Ω_m and Ω_Λ for the curved Λ CDM model by using different BAO data. The magenta contours are for the the combination of SDSS and 6dFGS BAO data by assuming $\Omega_b h^2 = 0.02227$, the cyan contours are for the the combination of SDSS and 6dFGS BAO data by assuming $\Omega_b h^2 = 0.02227$ and $h = 0.738$, the red contours are for the WiggleZ BAO data, the blue contours are for the combination of 6dFGS, SDSS and WiggleZ BAO data with free $\Omega_b h^2$ and h , and the shaded contours are for the BAO1 data with free $\Omega_b h^2$ and h . The dashed black line denotes the flat Λ CDM model.

$A(z)$ data presented in the WiggleZ, and we find that the result is similar. The result that the parameter $A(z)$ gives tighter constraint on Ω_m was also found in Gong et al. (2010); Gong, Wang & Cai (2010).

Recently, Busca et al. (2012) reported the detection of BAO in the Ly α forest of high-redshift quasars from the Baryon Oscillation Spectroscopic Survey. They found that $H(z = 2.3)r_s(z_d)/(1+z) = (1.036 \pm 0.036) \times 10^4$ km/s which gives the radial BAO data $\Delta z(z) = H(z)r_s(z_d)/c = 0.11404 \pm 0.00396$ at the redshift $z = 2.3$. In order to distinguish different BAO data, we refer the combination of 6dFGS, SDSS and WiggleZ BAO data as BAO. When the radial BAO data at $z = 2.3$ is added to the combination of 6dFGS, SDSS and WiggleZ BAO data, we call the data BAO1. With the addition of the radial BAO data at high redshift, we expect better constraints on the cosmological parameters. The 1σ and 2σ contours of Ω_m and Ω_k from BAO1 data are shown by the shaded regions in Fig. 2. We see that with the addition of BAO measurement at high redshift, the constraint on the curved Λ CDM model was greatly improved, and the constraint from BAO1 is even much better than that from SNe Ia data. These results suggest that more data points and more measurements at high redshift can help improve the results.

3.2 Modified holographic dark energy model

Apart from the simple Λ CDM model, we consider a specific dark energy model which just has one more parameter than Λ CDM model in this subsection. Applying the relationship between the mass and the horizon of a Schwarzschild black hole in higher dimensions and holographic principle, a modified holographic dark energy model (MHDE) with Hubble horizon as the ultraviolet cutoff was proposed in Gong & Li (2010). Both the DGP model (Dvali, Gabadadze & Porrati 2000) and Λ CDM model are special cases of this model, note that here we consider DGP model as an

effective dark energy model instead of a model which modifies gravity. In this model, Friedmann equation is (Gong & Li 2010; Dvali & Turner 2003)

$$E^2(z) - (1 - \Omega_m - \Omega_k - \Omega_r)E^{5-N}(z) = \Omega_k(1+z)^2 + \Omega_m(1+z)^3 + \Omega_r(1+z)^4, \quad (18)$$

where N is the spatial dimension. So we recover the DGP model if $N = 4$ and Λ CDM model if $N = 5$. This model has one more parameter than Λ CDM model, i.e., there are three model parameters $\mathbf{p} = (\Omega_m, \Omega_k, N)$ in this model in addition to the four nuisance parameter $(\alpha, \beta, \Omega_b h^2, h)$ to be fitted. For the flat MHDE model, $\Omega_k = 0$, we have only two model parameters Ω_m and N and we consider the constraints from SNe Ia data, the combination of SNe Ia and WMAP7 data, the combination of BAO and WMAP7 data, the combination of SNe Ia, BAO and WMAP7 data, and the combinations of all the observational data, the contours of Ω_m - N are shown in Fig. 3(a), and the 1σ constraints are summarized in Table 5. The constraints on N from BAO data alone are not good, so the results are not shown. Since BAO1 data alone gave much better constraint on the Λ CDM model, we also apply BAO1 data to the flat MHDE model and the result is shown in Fig. 3(a) by yellow contours. The constraints on N from BAO1 data alone are not good either, so the additional BAO measurement at $z = 2.3$ does not seem to help improve the constraint on the dynamics of dark energy, we mainly consider the effect of BAO data in the rest of the paper. In the upper left panel in Fig. 3, we use the following data: SNe data alone, BAO1 data alone, the combination of SNe and BAO data, the combination of SNe and WMAP7 data, the combination of BAO and WMAP7 data, and all the data combined.

Although BAO and BAO1 alone do not provide good constraints on N , the addition of BAO to SNe Ia data greatly improves the constraint on Ω_m , therefore improves the constraint on N . The effect of the WMAP7 data is similar except that the best-fitting values of the parameters Ω_m and N become smaller. The effect of the combination of BAO and WMAP7 data is similar to that of the combination of SNe Ia and WMAP7 data except that the best-fitting value of Ω_m becomes bigger and the best-fitting value of N becomes smaller. When we combine SNe Ia, BAO and WMAP7 data or all the observational data, the results are similar, so the addition of $H(z)$ has little effect. For all the combinations, $N \gtrsim 5$ at 1σ level. The SNLS3 SNe Ia data fitting parameters α and β are also consistent for different data combinations. These results show that both WMAP7 and BAO data help SNe data greatly improve the constraint on Ω_m , therefore improve the constraint on N . The degeneracy between Ω_m and N obtained from BAO data is different from that from WMAP7 data.

For the curved case, $\Omega_k \neq 0$, we have three model parameters. From the results of Λ CDM model, we see that the constraints on Ω_k from either SNe or BAO data alone are not good, and WMAP7 data help tighten the constraint on Ω_k . So in the curved model, we use WMAP7 data as priors. Therefore we only consider the combinations of SNe and/or BAO data with WMAP7 data for the curved model in the rest of this paper. The contours of Ω_m - N , Ω_m - Ω_k , and Ω_k - N are shown in Figs. 3(b)-(d), and the 1σ constraints are summarized in Table 5. In Figs. 3(b)-(d), we use the following data: the combination of SNe and WMAP7 data, the combination of BAO and WMAP7 data, the combination of SNe, BAO and WMAP7, and all the data combined. For the constraints on Ω_m and Ω_k , we see that the combination of BAO and WMAP7 data does better than the combination of SNe and WMAP7 data. However, for the constraint on N , both combinations get similar results. The degen-

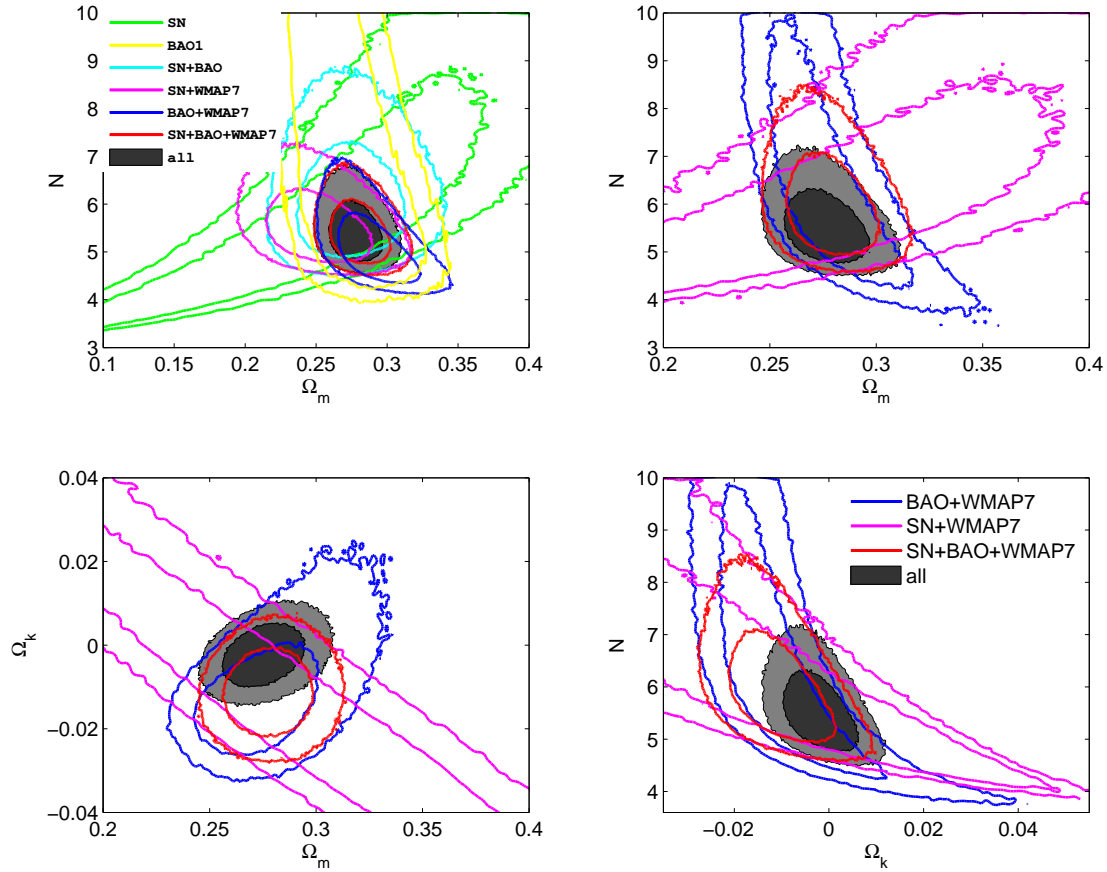


Figure 3. The marginalized 1σ and 2σ contour plots for MHDE model. The figures from the upper left to lower right are labeled as (a)-(d), respectively. (a) is for the flat MHDE model and (b)-(d) are for the curved MHDE model. In (a), we use the following data: SNe data alone, the combination of SNe and BAO data, the combination of SNe and WMAP7 data, the combination of BAO and WMAP7 data, the combination of SNe, BAO and WMAP7, and all the data combined. In (b)-(d), we use the following data: the combination of SNe and WMAP7 data, the combination of BAO and WMAP7 data, the combination of SNe, BAO and WMAP7, and all the data combined. The green lines label the constraints from SNe Ia data only, the yellow lines label the constraints from BAO1 data only, the cyan lines label the constraints from the combination of SNe Ia and BAO data, the magenta lines label the constraints from the combination of SNe Ia and WMAP7 data, the blue lines label the constraints from the combination of WMAP7 and BAO data, the red lines label the constraints from the combination of SNe Ia, BAO and WMAP7 data, and the shaded regions label the constraints from the combination of all the observational data.

eracies among the model parameters from the combination of SNe and BAO data and from the combination of BAO and WMAP7 data are different, so when we combine SNe, BAO and WMAP7 data, the constraints on the model parameters Ω_m , Ω_k and N are further improved. With the addition of $H(z)$ data, the best-fitting value of Ω_k is moved toward zero and the upper limit of N are reduced a little further. The results also show that observational data favour Λ CDM model more than DGP model since larger value of N is favored. The SNLS3 SNe Ia data fitting parameters α and β are consistent for different data combinations.

3.3 CPL parametrization

In this subsection, we apply the somewhat model-independent CPL parametrization (Chevallier & Polarski 2001; Linder 2003),

$$w(z) = w_0 + \frac{w_a z}{1+z}, \quad (19)$$

to test the effects of different combinations of data on constraining the property of dark energy. For the flat CPL model, we have three model parameters $\mathbf{p} = (\Omega_m, w_0, w_a)$. In Fig. 4, we show the marginalized 1σ and 2σ contour plots constrained from different combinations of data. The FOM from different data is shown in Fig. 5. The 1σ uncertainties of the model parameters are summarized in Table 6. Comparing the results from SNe Ia and BAO1 data, we see that BAO1 data give much better constraint on Ω_m , but their constraints on w_0 and w_a are much worse. Therefore BAO data cannot constrain the dynamics of dark energy although they give good constraints on Ω_m and the curved Λ CDM model. When the BAO data are added to the SNe Ia data, the uncertainty in w_a is reduced more than half and the FOM becomes 5 times larger. When WMAP7 data are added to the SNe Ia data, the uncertainty in w_a is reduced a little further and the FOM becomes almost 10 times larger. Compared the results from SNe data alone with those from the combination of BAO and WMAP7 data, we see that the SNe Ia data constrain better on w_0 and the combination of BAO and

Table 5. The marginalized 1σ constraints on MHDE model by different observational data. The top six rows are for the flat MHDE model and the bottom four rows are for the curved MHDE model.

Data	Ω_m	Ω_k	N
SNe	0.26 ± 0.09		$6.1^{+2.0}_{-1.8}$
SNe+BAO	$0.28^{+0.02}_{-0.03}$		$5.8^{+1.2}_{-0.5}$
SNe+WMAP7	$0.25^{+0.03}_{-0.02}$		$5.3^{+0.8}_{-0.3}$
BAO+WMAP7	0.29 ± 0.02		$4.9^{+0.8}_{-0.3}$
SNe+BAO+WMAP7	0.28 ± 0.01		$5.3^{+0.6}_{-0.3}$
All	0.28 ± 0.01		$5.3^{+0.6}_{-0.2}$
BAO+WMAP7	0.28 ± 0.02	-0.01 ± 0.01	$6.0^{+2.5}_{-1.0}$
SNe+WMAP7	$0.29^{+0.07}_{-0.08}$	-0.02 ± 0.03	$6.5^{+1.7}_{-1.5}$
SNe+BAO+WMAP7	$0.28^{+0.02}_{-0.01}$	-0.011 ± 0.007	$5.8^{+1.0}_{-0.5}$
All	0.28 ± 0.01	-0.003 ± 0.005	$5.5^{+0.6}_{-0.4}$

WMAP7 data constraints better on w_a ; the degeneracies among the model parameters from different data are different; both BAO and WMAP7 data help reduce the uncertainties in w_a ; and the help from WMAP7 data is a little better. The constraints on w_0 and w_a from the combination of SNe and WMAP7 data are much better than those from the combination of BAO and WMAP7 data, the FOM is almost 5 times larger. Note that we also fit two nuisance parameters α and β when we use SNe data, two nuisance parameters $\Omega_b h^2$ and h when we use BAO and WMAP7 data, four nuisance parameters ($\alpha, \beta, \Omega_b h^2, h$) when we combine SNe data with BAO and WMAP7 data. When the combined SNe Ia, BAO and WMAP7 data are used, we get better constraints on w_0 and w_a . The addition of $H(z)$ further reduces the uncertainties in w_0 and w_a . By using the constraints from the combination of all observational data, we reconstruct $w(z)$ and $Om(z)$ and the results are shown in Fig. 4. Λ CDM model is consistent with almost all the combinations of different data at the 1σ level.

For the curved CPL model, we have four model parameters $\mathbf{p} = (\Omega_m, \Omega_k, w_0, w_a)$, and we use the following data: the combination of SNe and WMAP7 data, the combination of BAO and WMAP7 data, the combination of SNe, BAO and WMAP7, and all the data combined. The 1σ and 2σ contours are shown in Fig. 6 and the upper panels of Fig. 7. The FOM from different data is shown in Fig. 5. The 1σ uncertainties of the parameters are summarized in Table 6. We see that the constraint on Ω_k from the combination of BAO and WMAP7 data (the blue lines) is better than that from the combination of SNe Ia and WMAP7 data (the magenta lines). The Ω_m - Ω_k contour becomes much smaller when we combine SNe Ia, BAO and WMAP7 data (the red lines). The addition of $H(z)$ further reduces the errors on Ω_k and moves the best-fitting value of Ω_k toward zero. From the w_0 - w_a contours in Fig. 6, we see that the constraints from the combination of SNe Ia and WMAP7 data are much better than those from the combination of BAO and WMAP7 data, and the FOM is almost 5 times larger. The uncertainties in w_a from the combination of SNe Ia, BAO and WMAP7 data are reduced more than half compared with those from the combination of SNe Ia and WMAP7 data, the FOM becomes more than 4 times larger. Although SNe Ia data do not provide tight constraints

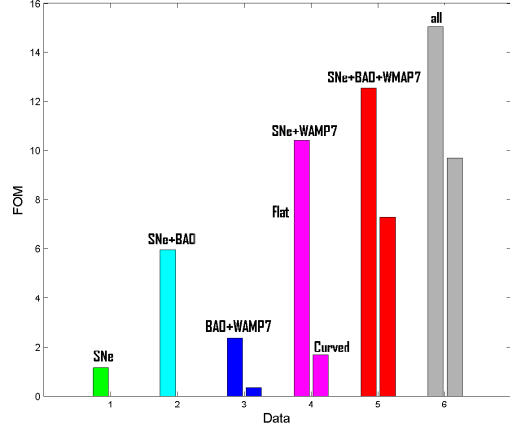


Figure 5. FOM versus different data combinations. The left bars are for the flat CPL model and the right bars are for the curved CPL model. For the curved CPL model, we use the following data sets: the combination of WMAP7 and BAO data, the combination of SNe and WMAP7 data, the combination of SNe, BAO and WMAP7 data, and all data combined. For the flat CPL model, we use two more data sets: SNe data alone, and the combination of SNe Ia and BAO data.

on Ω_m and Ω_k , their constraint on the equation of state parameter of dark energy is much better. Λ CDM model (the cross) is outside the 1σ contour when we use the combination of SNe Ia, BAO and WMAP7 data (the red lines). With the addition of $H(z)$ data, the w_0 - w_a contour is further reduced and Λ CDM model is inside the 1σ contour. By using the constraints from the combination of all observational data, we reconstruct $w(z)$ and the result is shown in Fig. 7.

From the above discussion, we find that both BAO and WMAP7 data help SNe data tighten the constraint on Ω_m , hence better constrains the other model parameters for the flat case. For the curved case, WMAP7 data help reduce the uncertainties in Ω_k , neither BAO nor WMAP7 data alone give good constraint on w_0 and w_a , but both WMAP7 data and BAO data help SNe Ia data break the degeneracies among the model parameters, hence tighten the constraint on the variation of equation of state parameter w_a , and WMAP7 data do the job a little better. SNLS3 SNe Ia data alone do not provide good constraints on Ω_m and Ω_k , but they provide good constrains on the parameters w_0 and w_a , especially on w_0 , so it is necessary to apply SNe Ia data to probe the dynamical property of dark energy. The addition of $H(z)$ data helps improve the constraints on the property of dark energy. Due to the degeneracies among the model parameters, we need to measure Ω_m and Ω_k more precisely in order to better probe the property of dark energy. In other words, we need to combine different observational data such as SNe Ia, BAO, WMAP7 and $H(z)$ data as long as the tensions among those data are not too big.

3.4 Piecewise parametrization of $w(z)$

Now we turn to probe the property of dark energy, we apply all the observational data outlined in section 2 to the piecewise parametrization of $w(z)$ for flat case,

$$\Omega_{DE}(z) = (1 - \Omega_m)(1+z)^{3(1+w_N)} \prod_{i=1}^N (1+z_{i-1})^{3(w_{i-1}-w_i)}, \quad (20)$$

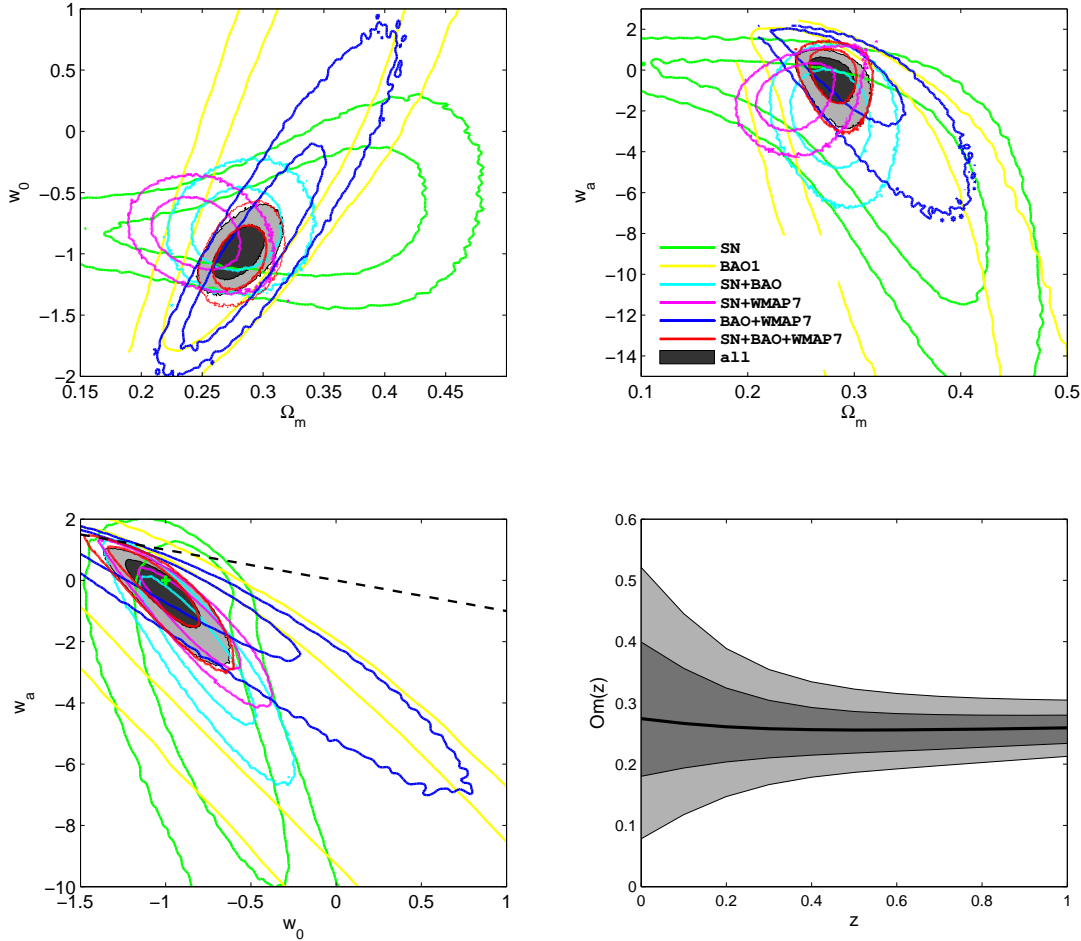


Figure 4. The marginalized 1σ and 2σ contour plots of Ω_m - w_0 , Ω_m - w_a and w_0 - w_a for the flat CPL model. The green lines label the constraints from SNe Ia data only, the yellow lines label the constraints from BAO1 data only, the cyan lines label the constraints from the combination of SNe Ia and BAO data, the magenta lines label the constraints from the combination of SNe Ia and WMAP7 data, the blue lines label the constraints from the combination of WMAP7 and BAO data, the red lines label the constraints from the combination of SNe Ia, BAO and WMAP7 data, and the shaded regions label the constraints from the combination of all the observational data. The dashed line in the w_0 - w_a contour denotes the condition $w_0 + w_a = 0$, and the + sign denotes the point corresponding to the Λ CDM model. In the lower right panel, we reconstruct $Om(z)$ by using the constraints from the combination of all data for flat CPL model, the solid line is obtained by using the best-fitting values of Ω_m , w_0 and w_a .

where $z_{i-1} \leq z < z_i$, $z_0 = 0$, $z_1 = 0.1$, $z_2 = 0.4$, $z_3 = 0.7$ and $z_4 = 1.4$. We also assume that $w(z > 1.4) = -1$. Following Huterer & Cooray (2005), we transform the parameters w_i to the de-correlated parameters \mathcal{W}_i . The results of \mathcal{W}_i are shown in the lower right panel of Fig. 7. The results are similar to those using Union2 SNe Ia data (Amanullah et al. 2010) and previous BAO data (Gaztanaga, Miquel & Sanchez 2009; Percival et al. 2010) in Gong, Zhu & Zhu (2011), and flat Λ CDM model is consistent with this result.

3.5 $q_1 - q_2$ parametrization

In this subsection, we reconstruct the deceleration parameter $q(z)$ with a simple two-parameter function (Gong & Wang 2007),

$$q(z) = \frac{1}{2} + \frac{q_1 z + q_2}{(1+z)^2}. \quad (21)$$

This parametrization recovers the matter dominated epoch at high redshift with $q(z) = 1/2$. The dimensionless Hubble parameter is

$$E(z) = \exp \left[\int_0^z [1 + q(u)] d \ln(1+u) \right] = (1+z)^{3/2} \exp \left[\frac{q_2}{2} + \frac{q_1 z^2 - q_2}{2(1+z)^2} \right]. \quad (22)$$

Since $E^2(z) \approx (1+z)^3 \exp(q_1 + q_2)$ when $z \gg 1$, so the role of matter energy density is played by the sum of the two parameters, $q_1 + q_2 = \ln \Omega_m$. Although Ω_m and Ω_k are not model parameters in this parametrization, the comoving distance depends on Ω_k through the function S_k , in order to better constrain the model parameters $\mathbf{p} = (q_1, q_2)$, we consider the flat case $\Omega_k = 0$ only. As discussed above for the CPL model, the flat assumption of $\Omega_k = 0$ may impose biased prior in the estimation of cosmological parameters due to the degeneracies among Ω_m , Ω_k and w (Clarkson, Cortes & Bassett 2007). However, the only effect of

Table 6. The marginalized 1σ constraints on CPL model by different observational data. The top six rows are for the flat CPL model and the bottom four rows are for the curved CPL model.

Data	Ω_m	Ω_k	w_0	w_a	FOM
SNe	$0.31^{+0.09}_{-0.07}$		$-0.8^{+0.4}_{-0.2}$	$-3.1^{+2.4}_{-5.9}$	1.15
SNe+BAO	$0.28^{+0.03}_{-0.02}$		$-0.83^{+0.26}_{-0.19}$	$-2.11^{+1.27}_{-1.95}$	5.94
SNe+WMAP7	$0.24^{+0.03}_{-0.02}$		-0.9 ± 0.2	$-1.1^{+0.8}_{-1.4}$	10.39
BAO+WMAP7	0.30 ± 0.04		$-0.81^{+0.58}_{-0.59}$	$-0.90^{+1.96}_{-1.91}$	2.38
SNe+BAO+WMAP7	$0.28^{+0.02}_{-0.01}$		$-1.12^{+0.27}_{-0.07}$	$0.32^{+0.21}_{-1.63}$	12.52
All	$0.28^{+0.02}_{-0.01}$		$-1.00^{+0.17}_{-0.13}$	$-0.33^{+0.53}_{-1.03}$	15.0
BAO+WMAP7	0.35 ± 0.07	-0.023 ± 0.013	0.4 ± 1.4	$-8.6^{+7.4}_{-7.2}$	0.36
SNe+WMAP7	$0.33^{+0.09}_{-0.06}$	$-0.03^{+0.02}_{-0.03}$	$-0.8^{+0.3}_{-0.2}$	$-3.4^{+2.1}_{-5.0}$	1.67
SNe+BAO+WMAP7	$0.28^{+0.02}_{-0.01}$	$-0.015^{+0.007}_{-0.008}$	-0.8 ± 0.2	$-2.02^{+1.35}_{-1.66}$	7.29
All	$0.28^{+0.02}_{-0.01}$	$-0.004^{+0.006}_{-0.007}$	$-0.97^{+0.27}_{-0.12}$	$-0.57^{+0.65}_{-1.86}$	9.69

Ω_k is through S_k , and $S_k(x) \approx x$ when Ω_k is small, so the impact of the flat assumption is expected to be small. Fitting this model to SNe data alone, we get the marginalized 1σ constraints $q_1 = -1.68^{+0.98}_{-0.87}$ and $q_2 = -1.06^{+0.19}_{-0.2}$. The contour plot is shown in Fig. 8(a). Using these results, we reconstruct $q(z)$ and $Om(z)$ and the results are shown in Figs. 8(b) and 8(c). So $q(z) < 0$ when $z \lesssim 0.5$ at 2σ level and flat Λ CDM model is consistent with the model at 1σ level. With the SNe Ia data alone, the evidence for current acceleration and past deceleration is very strong.

When we fit the model to BAO or WMAP7 data, we need to include the radiation-dominated era, and the nuisance parameters $\Omega_b h^2$ and $\Omega_m h^2$ which are not appeared in the model are just data fitting parameters, so we do not apply BAO and WMAP7 data alone. For approximation, we take the following Hubble parameter,

$$E^2(z) = \Omega_r(1+z)^4 + (1+z)^3 \exp \left[q_2 + \frac{q_1 z^2 - q_2}{(1+z)^2} \right], \quad (23)$$

where the current radiation component $\Omega_r = 4.1736 \times 10^{-5} h^{-2}$ (Komatsu et al. 2011). Fitting the model to the combined SNe Ia, BAO, WMAP7 and $H(z)$ data, we get the marginalized 1σ constraints, $q_1 = 0.20 \pm 0.13$ and $q_2 = -1.45 \pm 0.1$. The contour plot is shown in Fig. 8(a). Compared this result with that obtained from SNe Ia data alone, we find that they are inconsistent at 1σ model, this shows the tension between SNe Ia, BAO and WMAP7 data in fitting this model. Using the q_1 - q_2 contour, we reconstruct $q(z)$ and $Om(z)$ and the results are shown in Figs. 8(b) and 8(c). We find that $q(z)$ increases with the redshift and $q(z) < 0$ when $z \lesssim 0.5$ at 2σ level, the flat Λ CDM model is inconsistent with the model at 2σ level. These results may suggest that the approximation (23) is not good at high redshift. Since Ω_m does not appear in this model, the application of BAO and WMAP7 data may not be straightforward, this needs to be further studied.

3.6 Piecewise parametrization of $q(z)$

We also apply the piecewise parametrization to study the property of the deceleration parameter $q(z)$. For $z_{i-1} \leq z < z_i$, we have

$$E(z) = (1+z)^{1+q_N} \prod_{i=1}^N (1+z_{i-1})^{q_{i-1}-q_i}. \quad (24)$$

In this model, we have four parameters $\mathbf{p} = (q_1, q_2, q_3, q_4)$. We think this model approximates the behavior of $E(z)$ in the redshift range $z \lesssim 1.5$. In the radiation dominated era, we add the radiation contribution also. Again we follow Huterer & Cooray (2005) to transform the correlated parameters q_i to uncorrelated ones. Fitting the model to all observational data, we reconstruct the evolution of $q(z)$ and the results are shown in Fig. 8(d). Similar to that obtained by Union2 SNe Ia data (Gong, Zhu & Zhu 2011), we find that $q(z) < 0$ when $z \lesssim 0.6$ and $q(z) > 0$ at high redshift, so the evidences for current acceleration and past deceleration are very strong, and the transition redshift is around $z_t \sim 0.7$.

4 CONCLUSIONS

It is well known that BAO data are more sensitive to Ω_m and WMAP7 data are more sensitive to Ω_k . As more data points become available and the data become more accurate, we are able to constrain the cosmological parameters better. The constraints on Λ CDM model from SNe Ia data alone are similar to those from BAO data alone as shown in Figs. 1 and 2, the constraints on Ω_m by BAO data and the constraints on Ω_m and Ω_k by BAO1 data are even much better than those by SNe Ia data alone, and the addition of SNe data to the combination of BAO and WMAP7 data has little effect in improving the constraints of Ω_m and Ω_k . Applying BAO data to MHDE and CPL models, we find that the constraints on the dynamical behaviour of dark energy from BAO data alone are much worse than those from SNe Ia data alone. Although SNe Ia data alone are not able to provide good constraints on Ω_m and Ω_k , they provide much better constraint on the equation of state parameter of dark energy compared with that from BAO and WMAP7 data alone. Since the way that the model parameters are degenerated is different for SNe Ia, BAO and WMAP7 data alone, it is necessary to combine different data sets to get better constraint on the property of dark energy.

For the flat MHDE model, as shown in Fig. 3(a), although

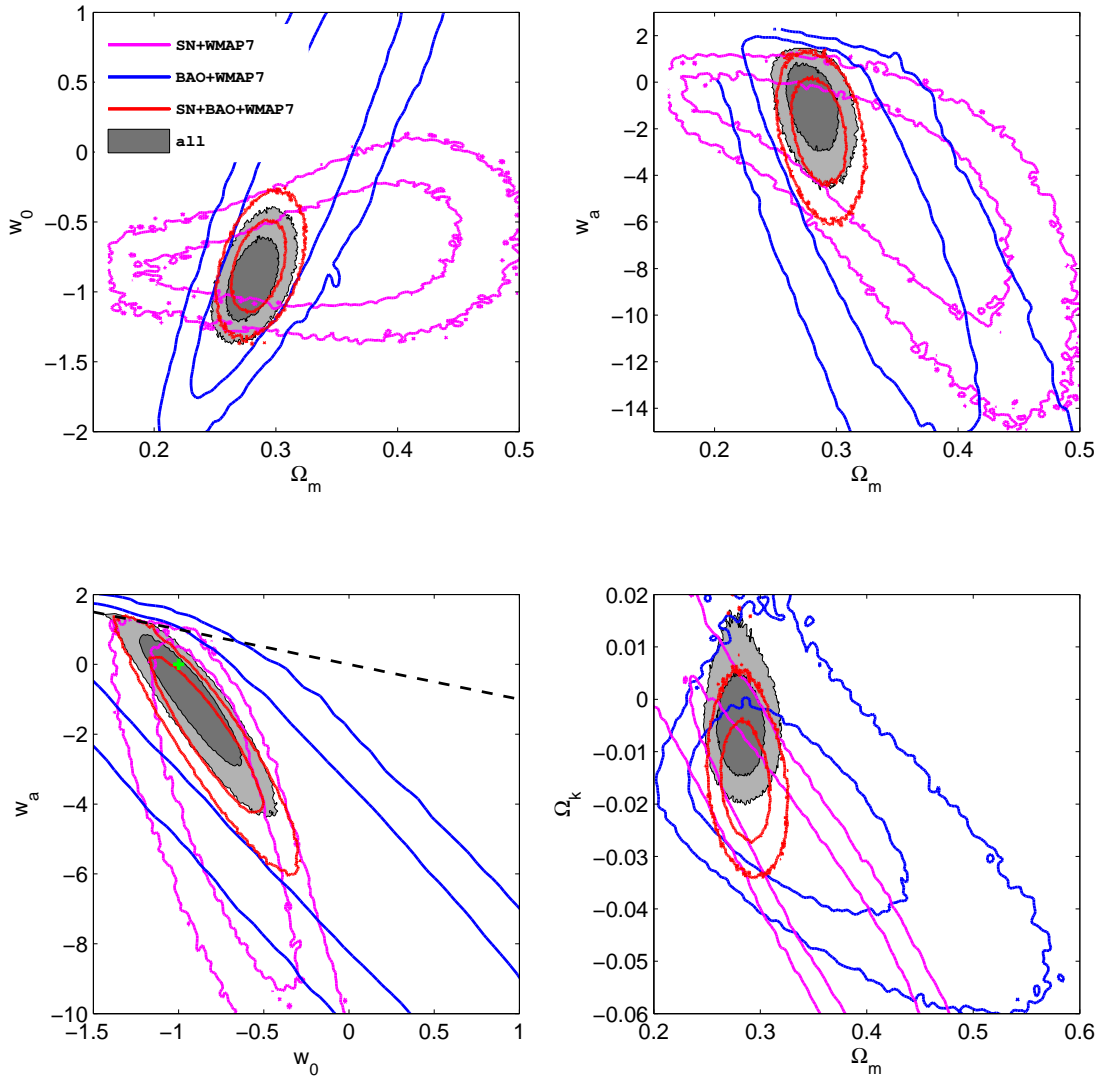


Figure 6. The marginalized 1σ and 2σ contour plots for the curved CPL model. the magenta lines label the constraints from the combination of SNe Ia and WMAP7 data, the blue lines label the constraints from the combination of WMAP7 and BAO data, the red lines label the constraints from the combination of SNe Ia, BAO and WMAP7 data, and the shaded regions label the constraints from the combination of all the observational data. The dashed line in the w_0 - w_a contour denotes the condition $w_0 + w_a = 0$, and the + sign denotes the point corresponding to the Λ CDM model.

BAO1 data provide good constraint on Ω_m , but the constraints on N are much worse, this suggests that BAO data alone are not able to constrain the dynamics of dark energy. Both WMAP7 and BAO data help SNe data greatly improve the constraint on Ω_m , and the help from WMAP7 is even a little greater. The constraints on Ω_m and N from the combination of BAO and WMAP7 are similar to those from the combination of SNe and WMAP7. The addition of $H(z)$ data to the combination of SNe Ia, BAO and WMAP7 data has little effect on improving the constraints. For the curved MHDE model, as shown in Figs. 3(b)-(d), the combination of BAO and WMAP7 data gives more stringent constraints on Ω_m and Ω_k than the combination of SNe and WMAP7 data does, but the constraints on N from both combinations are similar. The addition of $H(z)$

data helps tighten the constraints a little further. We also find that Λ CDM model is favoured against DGP model.

For the flat CPL model, as shown in Fig. 4, although BAO1 data provide good constraint on Ω_m , but the constraints on w_0 and w_a are much worse, this confirms that BAO data alone are not able to constrain the dynamics of dark energy. We get similar constraints on w_0 and w_a for SNe Ia data alone and the combination of BAO and WMAP7 data, although the constraints on Ω_m from the latter combination are much better. When the BAO data are added to the SNe Ia data, the uncertainty in w_a is reduced more than half and the FOM becomes 5 times larger as shown in Table 6 and Fig. 5. When WMAP7 data are added to the SNe Ia data, the uncertainty in w_a is reduced almost 4 times and the FOM becomes almost 10 times

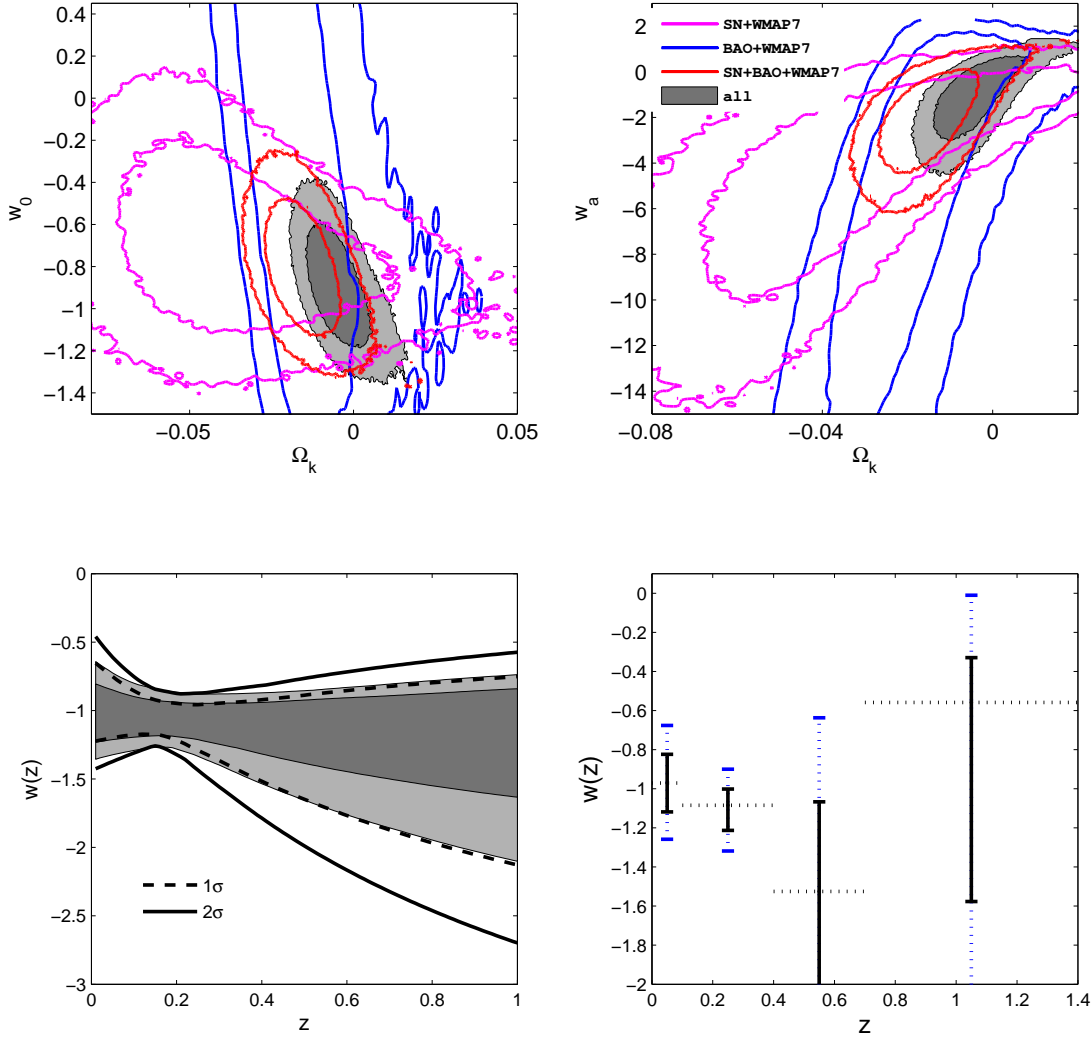


Figure 7. The marginalized 1σ and 2σ constraints from observations. In the upper panels, the magenta lines label the constraints from the combination of SNe Ia and WMAP7 data, the blue lines label the constraints from the combination of WMAP7 and BAO data, the red lines label the constraints from the combination of SNe Ia, BAO and WMAP7 data, and the shaded regions label the constraints from the combination of all the observational data. In the upper left panel, we show the Ω_k and w_0 contours for the curved CPL model. In the upper right panel, we show the Ω_k and w_a contours for the curved CPL model. In the lower left panel, we reconstruct the evolution of $w(z)$ by using the constraints from the combination of all data for CPL model, the shaded regions are for flat CPL model, and the black lines are for curved CPL model. The dashed and solid lines are for the 1σ and 2σ uncertainties, respectively. In the lower right panel, we show the observational constraints on $w(z)$ by using the piecewise parametrization, the solid and dashed lines are for the 1σ and 2σ uncertainties, respectively.

larger as shown in Table 6 and Fig. 5. Both BAO and WMAP7 data help SNe Ia data reduce the uncertainties in w_a , and the help from WMAP7 data is a little better. The addition of $H(z)$ data to the combination of SNe Ia, BAO and WMAP7 data has little effect on improving the constraints. Λ CDM model is consistent with all the observational data. This point is further supported by the reconstruction of $w(z)$ and $Om(z)$ as shown in Figs. 4 and 7.

For the curved CPL model, as shown in Figs. 6 and 7, we find that the combination of BAO and WMAP7 data gives better constraints on Ω_m and Ω_k than those from the combination of SNe Ia and WMAP7, but the constraints on w_0 and w_a from the first com-

binations are much worse than those from the latter combination. The 1σ uncertainties of w_0 and w_a from the latter combination are greatly reduced and the FOM becomes 5 times larger as shown in Table 6 and Fig. 5. The 1σ uncertainty of w_a is reduced more than half when we add BAO data to the combination of SNe Ia and WMAP7 data, and the FOM becomes more than 4 times larger as shown in Table 6 and Fig. 5. The 1σ uncertainty of w_a is reduced more than 5 times when we add SNe Ia data to the combination of BAO and WMAP7 data, and the FOM becomes more than 20 times larger as shown in Table 6 and Fig. 5. $H(z)$ data help move the best-fitting value of Ω_k towards zero and make the model more

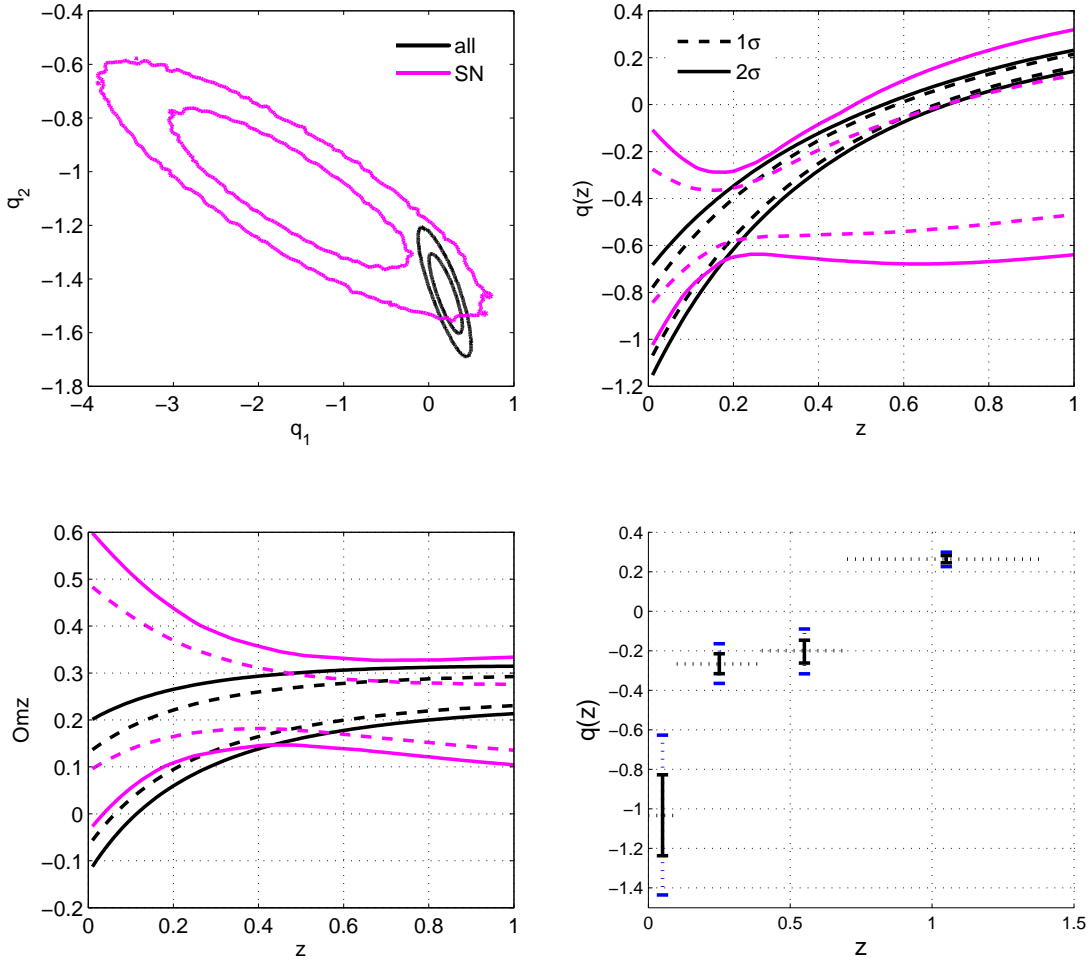


Figure 8. The marginalized 1σ and 2σ constraints on q_1 - q_2 parametrization and the piecewise parametrization of $q(z)$, the magenta lines represent the results obtained from SNe Ia data alone and the black lines represent the results obtained from all the observational data. The figures from upper left to lower right are labeled as (a)-(d), respectively. (a) shows the contour plots for q_1 and q_2 , (b) and (c) show the reconstruction of $q(z)$ and $\Omega_m z$, the dashed and solid lines in (b) and (c) represent the 1σ and 2σ uncertainties respectively, (d) shows the results for the piecewise parametrization of $q(z)$ constrained by all the observational data, the solid and dashed lines in (d) represent the 1σ and 2σ uncertainties respectively.

compatible with Λ CDM model. This effect of $H(z)$ which moves the best-fitting value of Ω_k towards zero for the curved Λ CDM, the curved MHDE and the curved CPL model seems to be general, this needs to be further studied.

To study the acceleration of the expansion of the Universe, we reconstruct the deceleration parameter $q(z)$ with a simple two-parameter function and the piecewise parametrization which approximates the evolution of the Universe in the redshift $z \lesssim 1.5$. For the SNe Ia data only, we see strong evidence that $q(z) < 0$ in the redshift $z \lesssim 0.5$ as shown in Fig. 8. The 1σ contour from SNe Ia data only is inconsistent with that from the combination of all data, it seems that there exists some tensions between SNe Ia data and other data; however, the inconsistency may come from the way we apply the BAO and WMAP7 data. Note that the nuisance model parameters $\Omega_m h^2$ and $\Omega_b h^2$ do not appear in the $q(z)$ parameterizations, but BAO and WMAP7 data depend on those parameters,

so we must be careful of applying those nuisance parameters, this needs to be further studied.

For the curved Λ CDM model, BAO1 data alone give much better constraint than SNe Ia data alone do, the combination of BAO and WMAP7 data constrains Ω_m and Ω_k much better than the combination of SNe and WMAP7 data. For the MHDE model, the constraints on the only dark energy parameter N from BAO or BAO1 data are much worse than those from SNe Ia data although the former data give much better constraints on Ω_m , the constraints on N from the combination of BAO and WMAP7 data are similar to those from the combination of SNe Ia and WMAP7 data, although the constraints on Ω_m and Ω_k from the former data are much better for the curved MHDE model. For the CPL model, we have two dark energy parameters w_0 and w_a . SNe Ia data alone give much better constraints on w_0 and w_a than BAO1 data alone do. The combination of SNe Ia and WMAP7 data give more stringent

contours of w_0 and w_a than the combination of BAO and WMAP7 data.

For the flat models, both BAO and WMAP7 data help SNe Ia data greatly improve the constraint on Ω_m and the help from WMAP7 is a little better, therefore both BAO and WMAP7 data help SNe Ia data tighten the constraint on the property of dark energy. The addition of $H(z)$ data to the combination of SNe Ia, BAO and WMAP7 data has little effect on improving the results. Although BAO and WMAP7 data provide reasonably good constraints on Ω_m and Ω_k , they are not able to constrain the dynamics of dark energy, we need SNe Ia data to probe the property of dark energy, especially the variation of the equation of state parameter of dark energy w_a . This point was well known due to the different directions of the degeneracy obtained from different data, here we confirm the point with the updated BAO data which constrain the Λ CDM model even better than SNe Ia data do. The addition of BAO data helps reduce the error on Ω_m and the addition of CMB data helps reduce the error on Ω_k , so both BAO and CMB data help SNe Ia data tighten the constraints on the property of dark energy due to degeneracies among Ω_m , Ω_k and $w(z)$, but neither data alone can be used to probe the dynamical property of dark energy. For the SNLS SNe Ia data, the nuisance parameters α and β are consistent for all different combinations of data. Their impacts on the fitting of cosmological parameters are minimal.

ACKNOWLEDGMENTS

This work was partially supported by the National Basic Science Programme (Project 973) of China under grant Nos. 2010CB833004 and 2012CB821804, the NNSF of China under grant Nos. 10935013 and 11175270, the Project of Knowledge Innovation Program (PKIP) of Chinese Academy of Sciences, Grant No. KJCX2.YW.W10, and the Fundamental Research Funds for the Central Universities.

REFERENCES

- Albrecht A., Bernstein G., Cahn R., Freedman W. L., Hewitt J., et al., 2006, preprint (arXiv: astro-ph/0609591)
- Amanullah R., Lidman C., Rubin D., Aldering G., Astier P., et al., 2010, *ApJ*, 716, 712
- Beutler F., Blake C., Colless M., Jones D. H., Staveley-Smith L., et al., 2011, *MNRAS*, 416, 3017
- Blake C., Kazin E., Beutler F., Davis T., Parkinson D., et al., 2011, *MNRAS*, 418, 1707
- Busca N. G., et al., 2012, preprint (arXiv: 1211.2616)
- Cai R.-G., Su Q., Zhang H.-B., 2010, *JCAP*, 1004, 012
- Chevallier M., Polarski D., 2001, *Int. J. Mod. Phys. D*, 10, 213
- Clarkson C., Cortes M., Bassett B. A., 2007, *JCAP*, 0708, 011
- Conley A., Guy J., Sullivan M., Regnault N., Astier P., et al., 2011, *ApJS*, 192, 1
- Dvali G., Turner M. S., 2003, preprint (arXiv: astro-ph/0301510)
- Dvali G., Gabadadze G., Porrati M., 2000, *Phys. Lett. B*, 485, 208
- Eisenstein D. J., Hu W., 1998, *ApJ*, 496, 605
- Gaztanaga E., Cabre A., Hui L., 2009, *MNRAS*, 399, 1663
- Gaztanaga E., Miquel R., Sanchez E., 2009, *Phys. Rev. Lett.*, 103, 091302
- Gong Y., Cai R.-G., Chen Y., Zhu Z.-H., 2010, *JCAP*, 1001, 019
- Gong Y., Li T., 2010, *Phys. Lett. B*, 683, 241
- Gong Y., Wang B., Cai R.-G., 2010, *JCAP*, 1004, 019
- Gong Y., Wu Q., Wang A., 2008, *ApJ*, 681, 27
- Gong Y., Zhu X.-M., Zhu Z.-H., 2011, *MNRAS*, 415, 1943
- Gong Y., Wang A., 2007, *Phys. Rev. D*, 75, 043520
- Hu W., Sugiyama N., 1996, *ApJ*, 471, 542
- Huang Q.-G., Li M., Li X.-D., Wang S., 2009, *Phys. Rev. D*, 80, 083515
- Huterer D., Cooray A., 2005, *Phys. Rev. D*, 71, 023506
- Kessler R., Becker A., Cinabro D., Vanderplas J., Frieman J. A., et al., 2009, *ApJS*, 185, 32
- Komatsu E., et al., 2011, *ApJS*, 192, 18
- Lampeitl H., Nichol R., Seo H., Giannantonio T., Shapiro C., et al., 2009, *MNRAS*, 401, 2331
- Lewis A., Bridle S., 2002, *Phys. Rev. D*, 66, 103511
- Li X.-D., Li S., Wang S., Zhang W.-S., Huang Q.-G., Li M., 2011, *JCAP*, 1107, 011
- Li Z., Wu P., Yu H., 2011, *Phys. Lett. B*, 695, 1
- Linder E. V., 2003, *Phys. Rev. Lett.*, 90, 091301
- Pan N., Gong Y., Chen Y., Zhu Z.-H., 2010, *Class. Quant. Grav.*, 27, 155015
- Percival W. J., et al., 2010, *MNRAS*, 401, 2148
- Perlmutter S., et al., 1999, *ApJ*, 517, 565
- Riess A. G., et al., 1998, *AJ*, 116, 1009
- Riess A. G., Macri L., Casertano S., Lampeitl H., Ferguson H. C., et al., 2011, *ApJ*, 730, 119
- Riess A. G., Strolger L.-G., Casertano S., Ferguson H. C., Mobasher B., et al., 2007, *ApJ*, 659, 98
- Sahni V., Shafieloo A., Starobinsky A. A., 2008, *Phys. Rev. D*, 78, 103502
- Serra P., Cooray A., Holz D. E., Melchiorri A., Pandolfi S., Sarkar D., 2009, *Phys. Rev. D*, 80, 121302
- Shafieloo A., Sahni V., Starobinsky A. A., 2009, *Phys. Rev. D*, D80, 101301
- Simon J., Verde L., Jimenez R., 2005, *Phys. Rev. D*, 71, 123001
- Stern D., Jimenez R., Verde L., Kamionkowski M., Stanford S. A., 2010, *JCAP*, 1002, 008
- Su Q., Tuo Z.-L., Cai R.-G., 2011, *Phys. Rev. D*, 84, 103519
- Sullivan M., Guy J., Conley A., Regnault N., Astier P., et al., 2011, *ApJ*, 737, 102